NRC Research Press

ARTICLE

Bio-grouting to enhance axial pull-out response of pervious concrete ground improvement piles

Hai Lin, Muhannad T. Suleiman, Hanna M. Jabbour, and Derick G. Brown

Abstract: Bio-grouting is an environmentallly friendly, sustainable, and low-cost ground improvement technique, which mainly utilizes microbial-induced carbonate precipitation. Previous large-scale applications of MICP have encountered practical difficulties including bio-clogging, which resulted in a limited zone of cemented soil around injection points. The research presented in this paper focuses on evaluating the feasibility of cementing a limited soil zone surrounding permeable piles using MICP bio-grouting to improve the mechanical response of permeable piles under axial pull-out loading. Two instrumented pervious concrete piles (test units), one with and one without MICP bio-grouting, were subjected to pull-out loading at the Soil-Structure Interaction Facility at Lehigh University. The pervious concrete pile served as an injection point during the MICP bio-grouting. The mechanical responses of the test units and surrounding soil were analyzed, along with shear wave (S-wave) velocities, moisture, and $CaCO_3$ contents of the surrounding soil. The results presented in this paper demonstrate that the limited MICP-improved zone, extending a radial distance of approximately 102 mm around pervious concrete piles, improved the load–displacement response, load transfer, and pile capacity under pull-out loading. The ratios between ultimate loads of the test units with and without MICP bio-grouting were 4.2. The average shaft resistance along the pile with MICP bio-grouting was up to 2.8 times higher than that of the pile without bio-grouting.

Key words: bio-grouting soil improvement, cementation, microbially induced carbonate precipitation (MICP), soil–pile interaction, pervious concrete.

Résumé : L'emploi de coulis de ciment biologique est une technique d'amélioration de sol respectueux de l'environnement, durable, à faible coût, qui utilise principalement la précipitation induite par des carbonates microbiens (MICP). Des applications précédentes à grande échelle de MICP ont rencontré des difficultés pratiques y compris le bio-encrassement, ce qui a donné lieu à une zone limitée du sol cimenté autour de points d'injection. La recherche présentée dans ce document porte sur l'évaluation de la faisabilité d'une zone de collage limitée des sols entourant des pieux perméables à l'aide deMICP bio-coulis afin d'améliorer la réponse mécanique de pieux perméables sous le chargement axial. Deux pieux en béton drainant instrumentés (unités d'essais), un avec et un sans coulis de ciment biologique par MICP, ont été soumis à un chargement d'arrachement au « Soil-Structure Interaction Facility » à l'Université Lehigh. Le pieu en béton drainant a servi de point d'injection pendant le traitement de coulis de ciment biologique par MICP. Les réponses mécaniques du sol environnant et des unités d'essai ont été analysées, en plus des vitesses d'onde de cisaillement (l'onde S), l'humidité et le contenu en $CaCO_3$ du sol environnant. Les résultats présentés dans cet article démontrent que la zone limitée d'amélioration par MICP, s'étendant d'une distance radiale d'environ 102 mm autour des pieux en béton drainant, a donné lieu à l'amélioration de la réponse de charge–déplacement, du transfert de charge, et de la capacité des pieux sous un chargement d'arrachement. Les rapports entre les charges ultimes des unités d'essai avec et sans coulis de ciment biologique par MICP étaient 4,2. La résistance de l'arbre moyen le long du pieu avec coulis de ciment biologique par MICP était jusqu'à 2,8 fois plus élevée que celui du pieu sans coulis. [Traduit par la Rédaction]

Mots-clés : amélioration du sol par coulis de ciment biologique, cimentation, précipitation induite par des carbonates microbiens (MICP), l'interaction sol–pieu, béton drainant.

Introduction

Post-grouting methods have been successfully utilized to increase shaft and (or) tip resistances of ground improvement and foundation systems (Gouvenot and Gabiax 1975; Bruce 1986*a*, 1986*b*; Plumbridge and Hill 2001). Constructing grouted foundations involves injecting pressurized grout through a proprietary system consisting of pipes that are attached to the steel cage and (or) a base grouting plate at the tip, creating a grouted zone along the shaft or below the tip (Plumbridge and Hill 2001; Ruiz and Pando 2009; Fattahpour at al. 2015). For drilled shafts, post-grouting has been successfully utilized to improve the tip resistance of foundations (Dapp and Mullins 2002; Mullins et al. 2006; Dapp and Brown 2010). However, application of grouting along the shaft of foundation systems is not commonly used due to the complex injection technique and difficult quality control (Joer et al. 1998; Thiyyakkandi et al. 2013; Fattahpour et al. 2015). To explore the possibility of bio-grouting, Lin et al. (2016*a*) presented an innovative grouted ground improvement pile alternative, bio-grouted permeable piles (pervious concrete piles), and this work focused on pile response when subjected to axial compression. This paper presents an innovative grouted ground improvement pile alternative, bio-grouted permeable piles (pervious concrete piles), and focuses on investigating their responses when subjected to axial pull-out loading.

Received 10 August 2016. Accepted 27 June 2017.

H. Lin and H.M. Jabbour. Mueser Rutledge Consulting Engineers, 225 W. 34th St., New York, NY, 10122, USA.
M.T. Suleiman and D.G. Brown. Lehigh University, 1 W. Packer Ave., Bethlehem, PA 18015, USA.
Corresponding author: Muhannad T. Suleiman (email: mts210@lehigh.edu).

The bio-grouting process offers a potential cost-effective and lower environmental-impact solution to enhance the response of ground improvement and foundation systems (Ivanov and Chu 2008; Suer et al. 2009). Currently, most studies are on a bio-grouting process that relies on the microbially induced carbonate precipitation (MICP) process to induce calcium carbonate ($CaCO_3$) precipitation (Stocks-Fischer et al. 1999; Ivanov and Chu 2008; van Paassen 2009; Mortensen et al. 2011; Burbank et al. 2013; DeJong et al. 2013; Lin et al. 2016*a*, 2016*b*). The MICP grouting process can realize outcomes similar to cement-based grouting along the shaft and at the tip of permeable piles, while using a simple percolation process (Lin et al. 2015, 2016*a*). In addition, enhancing the mechanical response of permeable piles using MICP bio-grouting requires only a limited zone of soil improvement around the pile, mitigating the practical difficulty of bio-clogging encountered in mass soil stabilization using MICP (van Paassen et al. 2010; Cheng and Cord-Ruwisch 2013).

Background

There are many practical applications where foundation systems are subjected to pull-out loading, including transmission towers, jetties, and mooring systems for ocean surface and submerged platforms (Gouvenot and Gabiax 1975; Vanitha et al. 2007). Post-grouting has been utilized to improve the performance of foundations subjected to axial loading as well as their safety and economy (Gouvenot and Gabiax 1975; Joer et al. 1998). However, post-grouting was mainly utilized to enhance the tip resistance of foundations, with very limited cases where post-grouting was utilized to improve the shaft resistance due to the complex pressurized injection technique, difficult quality control, and proprietary systems (Joer et al. 1998; Thiyyakkandi et al. 2013; Fattahpour et al. 2015). This paper focuses on bio-grouting of permeable piles to improve the shaft resistance utilizing simple percolation injection.

Bio-grouted pervious concrete pile alternative

Pervious concrete is a special single-size aggregate concrete that offers high porosity and permeability (Suleiman et al. 2014). Based on the experimental results, the axial-compression behavior of pervious concrete piles showed higher strength and stiffness than that of an identical granular column, while having a similar permeability coefficient (Suleiman et al. 2014; Ni et al. 2016). The high permeability of pervious concrete piles allows for easy grouting along the pile shaft and at the tip of the pile using percolation of a low viscosity bio-grout without the need of using complex proprietary pressure injection systems.

MICP bio-grouting involves a microbially regulated process of $CaCO_3$ precipitation to cement soil particles and clog pore space. This process improves strength, stiffness, and volume-dilatancy, and reduces permeability of the soil matrix (Ferris et al. 1996; Stocks-Fischer et al. 1999; DeJong et al. 2006; Whiffin et al. 2007; Al Qabany and Soga 2013; Soon et al. 2014; Montoya and DeJong 2015; Lin et al. 2016*b*). The bio-grouted pervious concrete pile alternative avoids bio-clogging around injection points, which limits MICP use for mass stabilization, and focuses on improving a limited zone (or $CaCO_3$ cemented zone) along the pile, enhancing the response of the bio-grouted pile system when subjected to axial pull-out loading.

Financial and environmental impact of MICP bio-grouting

Studies comparing MICP bio-grouting with jet or chemical grouting showed that bio-grouting is more cost effective with a lower environmental impact than jet grouting (Ivanov and Chu 2008; Suer et al. 2009). Suer et al. (2009), who carried out a life cycle assessment on a real project to analyze the environmental and economic impacts of MICP and jet grouting, concluded that the total energy used for MICP (3 GJ per m^3 of soil) was half of that used for jet grouting (6 GJ/m^3 of soil) with MICP costing 55% of jet grouting. This difference is mainly attributed to the use of heavier equipment, large amount of spoil waste, and related transportation of jet grouting. It was also noted that the byproducts of MICP bio-grouting (e.g., ammonium cation and chloride ion with high pH of approximately 9) might affect groundwater and soil ecosystem, which still lack more thorough investigations.

Objectives and methodology

The objective of this paper is to evaluate the use of bio-grouting for enhancing the response of permeable foundations subjected to axial pull-out loading. To achieve this goal, two instrumented pervious concrete pile tests were performed at the Soil-Structure Interaction Facility at Lehigh University. Test No. 1 was performed without MICP bio-grouting and test No. 2 used MICP bio-grouting. The pile and surrounding soil were instrumented using strain gauges and bender elements. The responses of the pile and surrounding soil with and without MICP bio-grouting were analyzed and compared. At the conclusion of the tests, soil samples were analyzed for moisture and $CaCO_3$ contents, and crystal formation was characterized at the particle scale using scanning electron microscopy (SEM).

Materials and preparation methods

Soil properties

Bar sand was used for both pile laboratory tests. Based on the particle-size distribution curve (Fig. 1*a*), Bar sand was classified as poorly graded fine sand (SP) using the Unified Soil Classification System (ASTM 2011). The minimum and maximum unit weights of oven-dried bar sand were 14.54 and 16.75 kN/m^3, respectively (maximum void ratio of 0.79 and a minimum void ratio of 0.55) (ASTM (2009*a*) standard D4253 and ASTM (2009*b*) standard D4254). The sand placed in the soil box had an average unit weight of 15.1 kN/m^3, relative density of 29%, and water content of 0.4%, which were measured by a nuclear density gauge.

A series of consolidated drained (CD) triaxial tests with different confining pressures (25, 50, and 100 kPa) were performed to characterize the mechanical properties of the sand without MICP bio-grouting treatment. Furthermore, a CD triaxial test was performed on a sample with MICP bio-grouting treatment at a confining pressure of 100 kPa. The triaxial specimens (70 mm diameter, length to diameter ratio: 2:1) were prepared at the same relative density as the sand in the soil box. The MICP treatment procedure from Lin et al. (2016*b*) with 0.3 mol/L $CaCl_2$ was utilized for the test. This process resulted in an average $CaCO_3$ content of 1.3%. The measured deviator stress–axial strain and volume change during the CD triaxial tests are presented in Fig. 1*b*. (Note that the test for MICP-treated sample was stopped at axial strain of 3.5%.) The initial soil modulus (E_i) of the sand without treatment was evaluated as a function of confining pressure (σ_3) as $E_i = kP_a(\sigma_3/P_a)^n$ (Janbu 1963), where P_a is the atmospheric pressure of 100 kPa and k and n were calculated to be 401.6 and 0.48, respectively (Fig. 1*b*). The K_f line presented in Fig. 1*c* indicates that the peak friction angle of the bar sand without MICP treatment was 38°. The peak strength of MICP-treated specimen was 21% higher than that of the untreated specimen at the same confining pressure. Volumetric strain of sand without MICP treatment revealed contraction followed by dilation. This dilation at low relative density could be attributed to the low confinement pressure applied during triaxial tests. It is observed that MICP treatment significantly increased the dilatancy of sand. The MICP-treated specimen experienced less contraction at small strains followed by more dilation at larger strains than the untreated specimens. The observed response for MICP-treated sample is similar to the results reported by Feng and Montoya (2015), Montoya and DeJong (2015), and Lin et al. (2016*b*). These researchers also concluded that the shear strength of soil increases with higher $CaCO_3$ content.

Fig. 1. Material properties: (*a*) gradation of soil used in the test box; (*b*) stress–strain and volumetric strain of sand samples without bio-grouting under consolidated drained (CD) triaxial tests; (*c*) p'_f–q_f diagram at peak stresses of soil samples. E_i, initial soil modulus; K_f, stress path line at failure; p'_f and q_f, Lambe mean and deviatoric stress path parameters at failure, respectively; σ_3, confining pressure; σ'_1 and σ'_3, major and minor effective principal stresses, respectively; ϕ, friction angle. [Colour online.]

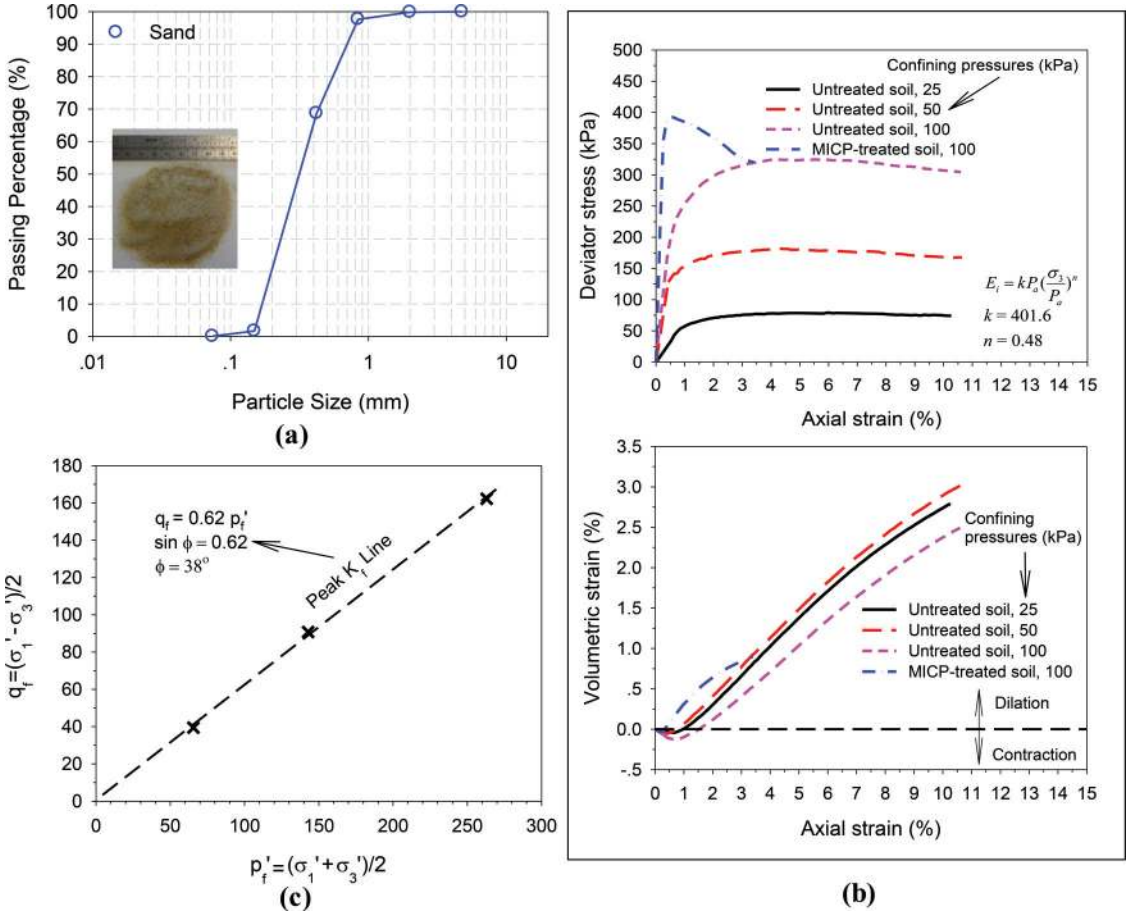

Pervious concrete properties

Cylindrical pervious concrete samples were used to measure the porosity, permeability, compressive strength, and split tensile strength. The compressive strength was determined using ASTM (2009*c*) standard C39, the permeability was measured using a falling-head permeameter (built in-house), the porosity was measured using ASTM (2009*d*) standard C1688, and the split tensile strength was measured using ASTM (2009*e*) standard C496. The pervious concrete samples had an average porosity of 19%, a permeability coefficient of 0.3 cm/s, a 28 day compressive strength of 18.5 MPa, and a split tensile strength of 1764 kPa. These properties are similar to those reported by Suleiman et al. (2014) and Ni et al. (2016).

Bacteria preparation and MICP recipes

The bacterial strain *Sporosarcina pasteurii* (*S. pasteurii*, ATCC 11859) was used for the pile tests. A stock culture of *S. pasteurii* was inoculated into 0.2 μm filter-sterilized growth media (10 g yeast extract and 5 g ammonium sulfate in 500 mL 0.13 mol/L Tris Buffer at pH = 9.0) until the optical density at 600 nm (OD_{600}) reached 0.8~1, corresponding to a bacteria density of ~1.5×10^7 cells/mL. The bacteria were then harvested and centrifuged at 4000*g*. The bacteria were stored at 4 °C until used. Additional details on the bacterial preparation are available in Lin et al. (2016*a*).

The solutions used for bio-grouting include urea medium (20 g urea, 2.12 g $NaHCO_3$, 20 g NH_4Cl, and 3 g nutrient broth in 1 L deionized water at pH = 6) and cementation medium (urea medium with 300 mmol/L $CaCl_2$) to induce $CaCO_3$ precipitation. Before MICP bio-grouting treatment, bacteria were suspended into urea medium at a bacteria density of 5×10^7 cells/mL. The treatment procedure is discussed in further details later in the paper.

Testing facility and instrumentation

A test soil box with dimensions of 1.1 m × 1.1 m × 1.2 m was utilized for the two axial pull-out load tests. The setup of the tests and detailed instrumentation are shown in Figs. 2 and 3. For both tests, one pervious concrete pile with a diameter of 76 mm and a length of 1.08 m was cast and utilized. Pile length of 927 mm was embedded in sand (Fig. 2). A threaded rebar (9.5 mm in diameter) was placed along the center of the pile during concrete casting for strain gauge measurement and pile attachment to the load cell. When comparing the pile diameter (B = 76 mm) to the mean sand particle size (d = 0.3 mm) used in the experiments, the ratio of B/d equals to 253. Given that the B/d ratio is larger than 40 (B/d ratio beyond which no scaling is required for soil particles ranges from 15 to 40 as reported by Ovensen 1979 and Nunez 1988), the research team did not scale the soil particle size in the tests.

The 1g large laboratory scale model test was scaled using the approach suggested by Altaee and Fellenius (1994). To represent field-scale conditions (prototype) with larger pile size and higher confinement stress, this approach relies on geometric scaling, stress scaling as well as void ratio scaling. The stress and void ratio scaling use the mean principal stress (log scale) — void ratio line parallel to the critical state line (called steady state line by Altaee and Fellenius 1994, Been and Jefferies 1985, and Ishihara et al.

Fig. 2. Instrumentation for two pull-out loading tests: (*a*) side view; (*b*) top view. [Colour online.]

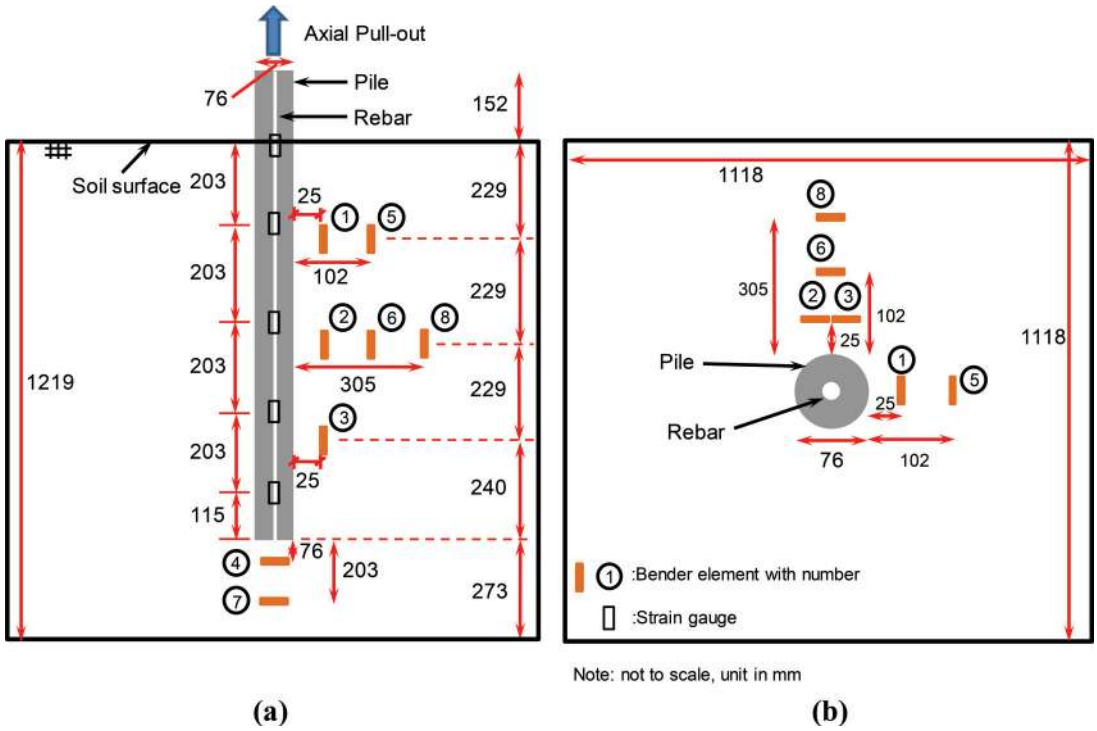

Fig. 3. Instrumentation, microbially induced carbonate precipitation (MICP) bio-grouting and pull-out loading setup: (*a*) soil raining; (*b*) bender element installation; (*c*) media injected from the top of the pile; (*d*) pull-out loading setup. [Colour online.]

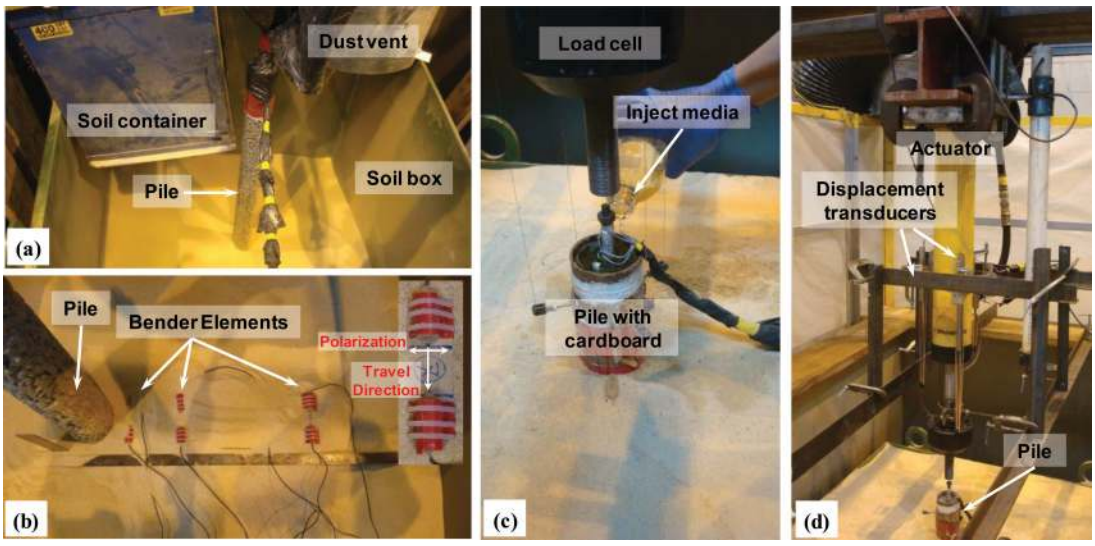

1991). In this approach, it is assumed that model conditions (mean principal stress versus void ratio) on a line parallel to the critical state line correctly simulate a prototype condition on the same line.

For our experiment, a geometric scaling ratio of 4.5 was used assuming a prototype permeable ground improvement foundation system (pervious concrete ground improvement pile) with a diameter of 340 mm and a length of 4.50 m. A scaling ratio of 4.5 of mean principle stress was also used. Accordingly, a prototype overburden pressure of ~78 kPa with void ratio of 0.58 were scaled to a model overburden pressure of ~16 kPa with a void ratio of 0.72.

During the test preparation, the pile was attached to the load cell first as shown in Fig. 3*a*. The bar sand was then rained into the soil box using the soil raining system (Lin et al. 2015; Ni et al. 2016). As shown in Fig. 2*a*, five strain gauges were installed along the threaded rebar at depths of 0, 203, 406, 609, and 812 mm below the soil surface.

Bender elements were installed in the soil box to monitor shear wave (S-wave) velocities during MICP bio-grouting treatment and during loading. Bender elements were fabricated in-house using piezo elements (4 mm × 8 mm parallel type-PSI–5H4ET226-H4–303Y from Piezo Systems, Inc.). The piezo element was embedded in nylon set screw (diameter of 12.7 mm and length of 25 mm) with 3 mm tip that was coated by waterproof epoxy (Devcon High-Strength 5 Minute Epoxy). As shown in Fig. 3*b*, a pair of bender elements was fixed on a very thin wooden piece to match the vibration direction (e.g., polarization) between both sensors en-

Table 1. Summary of MICP bio-grouting procedure and S-wave velocity monitoring schedule.

Injection No.	Action	Time (h)	Urea medium with bacteria (L)	Cementation medium (L)
1	Measure initial V_s	0	—	—
	Measure V_s	0.25	1.5	1.5
		0.6	1.5	1.5
		0.98	1.5	1.5
2	Measure V_s every hour	12	—	8
3	Measure V_s every 2 h	24	—	8
4	Measure V_s every 6 h	50	1.5	1.5
Total			6	22

Note: V_s, S-wave velocity.

Fig. 4. S-wave velocities and infiltration rate versus time during MICP bio-grouting of test No. 2. V_s, S-wave velocity. [Colour online.]

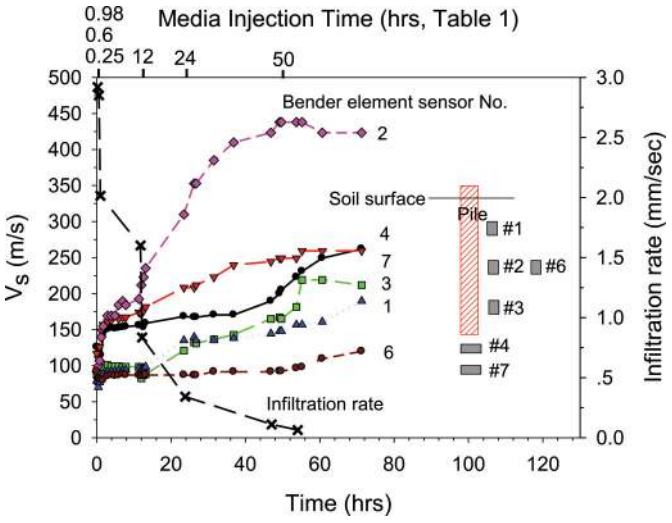

abling horizontally transmitted S-wave velocity with horizontal polarization. The bender elements data acquisition and interpretation system was discussed in detail by Lin et al. (2016*b*). As shown in Fig. 3*b*, bender elements sensor Nos. 2, 6, and 8 were placed at soil depth of 458 mm and at distances of 25, 102, and 305 mm from the pile surface. Bender element sensor Nos. 1 and 5 were installed at soil depth of 229 mm and distance of 25 and 102 mm from the pile. Bender element sensor No. 3 was installed at soil depth of 687 mm and distance of 25 mm from the pile. Bender element sensor Nos. 4 and 7 were installed at 76 and 203 mm below the tip of the pile.

Experimental procedures

MICP bio-grouting

After raining the sand, the pile was detached from the load cell and the top of the pile was wrapped with cardboard (Fig. 3*c*). For test No. 1 (without MICP bio-grouting), 16 L deionized water was percolated from the top of the pile to achieve similar soil moisture content around the pile in both tests. For test No. 2 (with MICP bio-grouting), urea medium with bacteria and cementation medium were percolated into the pile by following the detailed procedure summarized in Table 1. During the media injection, the infiltration rates were monitored following ASTM (2009*f*) standard C1701. S-wave velocities were also monitored during the whole MICP bio-grouting process as shown in Table 1.

Loading procedure

After the deionized water injection or MICP bio-grouting treatment, the cardboard was removed and the actuator was connected to the pile. Four displacement transducers were installed to measure the pull-out displacement at the top of the pile (Fig. 3*d*). The two axial pull-out tests were conducted in accordance with the fast procedure outlined in ASTM (2009*g*) standard D3689. During the test, loading at each increment was held constant for at least 4 min or until the pile head displacement stabilized. The tests were stopped when the displacement at the pile head continued increasing without an increase of the applied load. For test No. 1 (without bio-grouting), a load increment of 22.2 N was used for loads until 150 N and a load increment of 44.5 N was used for larger loads. For test No. 2 (with MICP bio-grouting), load increments of 44.5 and 89 N were used for loads until 932 and 3879 N, respectively.

Fig. 5. S-wave velocities profile versus time during MICP bio-grouting in test No. 2: (*a*) at different soil depths; (*b*) at soil depth of 458 mm, but at different distances from the pile. [Colour online.]

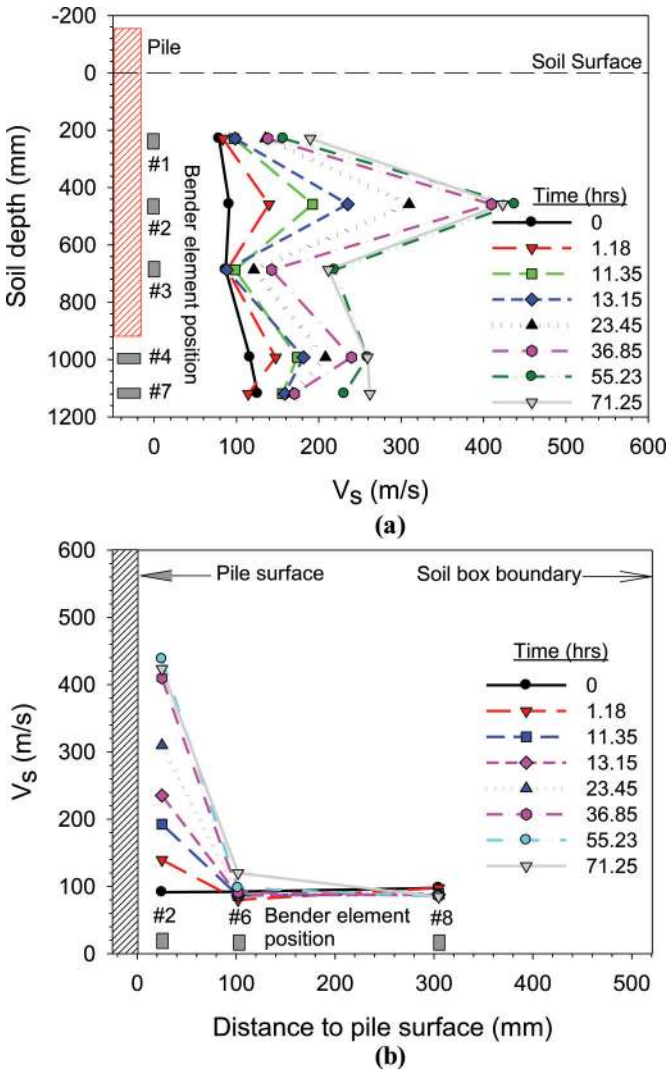

Moisture and calcium carbonate contents measurement

After the pull-out loading tests, soil samples were collected across the soil box. A total of 40 and 270 soil samples (each sample weight ~30 g) from test Nos. 1 and 2, respectively, were collected. Samples from test Nos. 1 and 2 were dried, which were used to measure the moisture content. The samples from test No. 2 were then mixed with 20 mL of 5 mol/L hydrochloric acid to measure the Ca^{2+} concentration (C_{Ca} (g/mL)) using atomic absorption spectroscopy and the measured Ca^{2+} concentration was used to calcu-

Fig. 6. (*a*) Soil surface in test No. 2 during pull-out loading; (*b*) vertical load versus displacement at the top of the pile. [Colour online.]

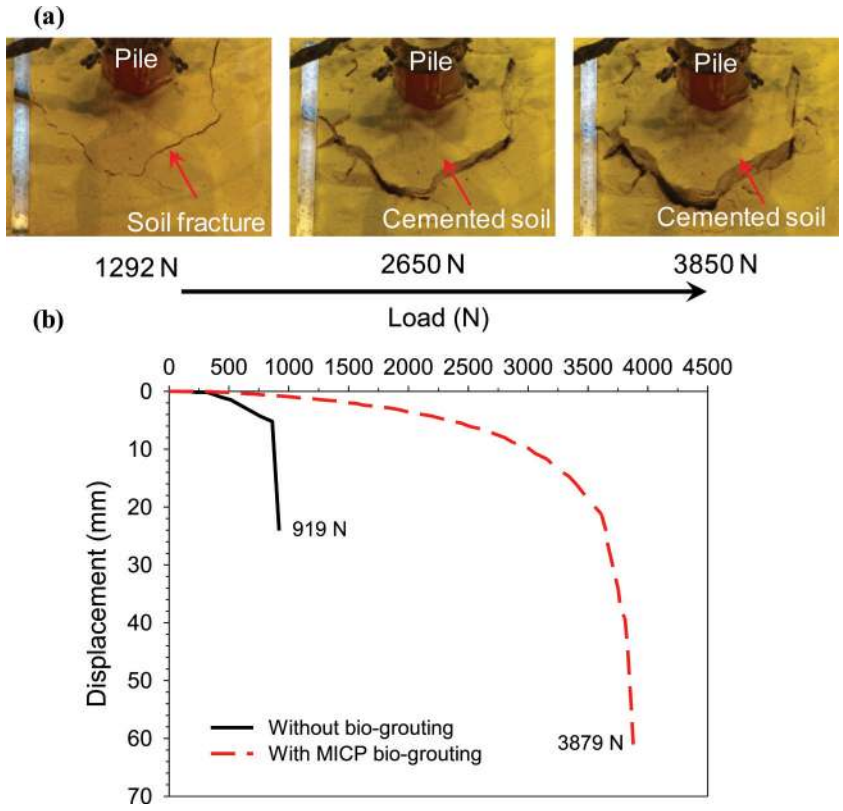

late the $CaCO_3$ content. The detailed procedure of calcium carbonate content calculation can be found in Lin et al. (2016*a*, 2016*b*). In addition, SEM-energy dispersive spectroscopy (SEM-EDS, Environmental SEM FEI XL30) was used to characterize crystal formation of $CaCO_3$ in the soil samples.

Results

S-wave velocities during MICP bio-grouting

The results of the S-wave velocities measurements during MICP bio-grouting are shown in Fig. 4. Bender element Nos. 1 to 3 were installed 25 mm from the pile surface and at depths below the soil surface of 229, 458, and 687 mm, respectively. Bender element Nos. 4 and 7 were installed at 76 and 203 mm below the pile tip. Sensor No. 6 was located at depth of 458 and 102 mm distance from the pile surface.

The original S-wave velocities before MICP bio-grouting treatment, which were measured and shown at time of 0 h, range from 78 to 126 m/s at different depths. After the first injection between 0.25 and 0.98 h, the S-wave velocities measured by sensor Nos. 2, 4, and 7 show immediate increases, indicating $CaCO_3$ cementation at the sensors' locations. While the S-wave velocities of sensor Nos. 1, 3, and 6 showed small or no increases, indicating less $CaCO_3$ cementation at their locations. The S-wave velocity measured by sensor No. 2 continued to increase after the media injections at 12 and 24 h (Table 1), and then reached a plateau at 430 m/s after media injection at 50 h.

The comparisons of the S-wave velocities measured from sensor Nos. 4 and 7 (located below the tip of the pile) show that the S-wave velocity of sensor No. 4 increased faster between 12 and 38 h, whereas after 38 h, the S-wave velocity of sensor No. 7 increased faster. This could be attributed to the bacteria, urea, $CaCl_2$ media flow path from the pile tip to the soil, which induced $CaCO_3$ cementation first at the position of sensor No. 4 and then No. 7. At the end of the MICP bio-grouting treatment (72 h), the S-wave velocities measured by sensor Nos. 4 and 7 reached similar S-wave velocities of 260 m/s. S-wave velocities of sensor Nos. 1 and 3 showed similar variation before 35 h. After 35 h, the S-wave velocity of sensor No. 3 showed a much higher increase rate than that of sensor No. 1, and then followed by reaching a plateau at the end of the bio-grouting treatment. The S-wave velocity of sensor No. 1 after 35 h showed a slower increase rate than that of sensor No. 3; however, it continued increasing until the end of the bio-grouting treatment without showing a plateau. The S-wave velocity of sensor No. 6, located 102 mm away from the pile, showed almost no change before 50 h and then followed by an increase by only 30% till the end of the treatment. Sensor Nos. 5 and 8 did not show clear change of S-wave velocities during the MICP bio-grouting, indicating that bio-grouting extended to a radial distance of approximately 102 mm (distance to bender element Nos. 5 and 6) around the pile.

At the end of the MICP bio-grouting treatment, all sensors showed S-wave velocity plateaus, except sensor Nos. 1, 6, and 7 (Fig. 4). This could be attributed to bio-clogging along most of the test pile, reducing the flow rate of the media solution out of the pile and minimizing or limiting the production of $CaCO_3$ cementation at the sensors locations. The observed bio-clogging was also confirmed by the low infiltration rates after 50 h as will be discussed in the next paragraph. At the end of the MICP bio-grouting (72 h), the S-wave velocities of sensor Nos. 1, 2, 3, 4, 6, and 7 had increased by an average of 1.5 times. It is important to note that the S-wave velocities of test No. 1 (without MICP bio-grouting) during deionized water injection were constant, which are similar to the measured S-wave velocities of test No. 2 before MICP bio-grouting treatment with a maximum difference of 22 m/s between the two tests.

Equation 1 was used to calculate the infiltration rate (ASTM 2009*f*):

Fig. 7. Characteristics of the piles and surrounding soil of two pull-out tests: piles and soil surface in (*a*) test No. 1 and (*b*) test No. 2 after pull-out loading; excavated piles of (*c*) test No. 1 and (*d*) test No. 2 after pull-out test. [Colour online.]

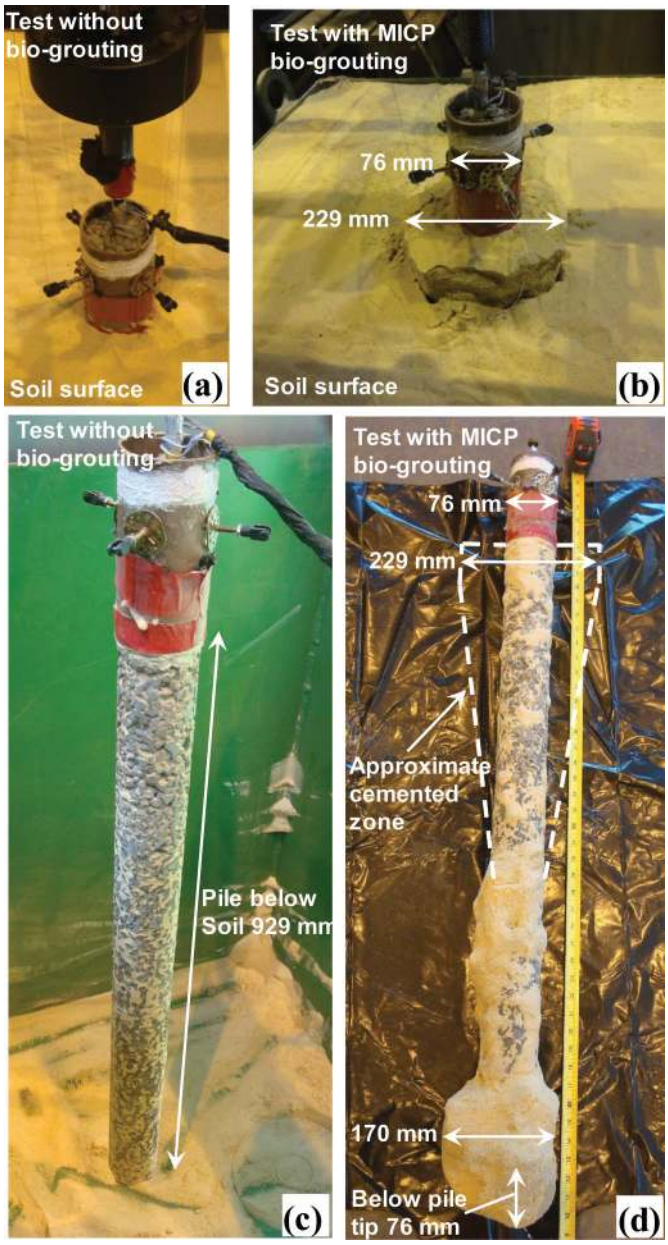

$$I = \frac{KM}{(D^2 t)} \quad (1)$$

where I is the infiltration rate (mm/s), K is a constant parameter (4 583 666 000 (mm^3·s)/(kg·h) according to ASTM (2009*f*)), M is the mass of the infiltrated solution (kg), D is the diameter of infiltration cylinder (i.e., the pile in our case, mm), and t is the time required for measured amount of solution to infiltrate the concrete pile(s). As seen in Fig. 4, the infiltration rate decreased from 2.9 mm/sec before the MICP bio-grouting to 0.06 mm/sec at the end of bio-grouting (i.e., 98% reduction), indicating the initiation of bio-clogging in the sand matrix around the pile. In addition, the observed bio-clogging was also confirmed by the plateau of most measured S-wave velocities at the end of the MICP bio-grouting.

Fig. 8. Comparison of (*a*) load transfer along pile length of both tests at different loading stages and (*b*) averaged interface friction stress versus displacement at the top of the pile. [Colour online.]

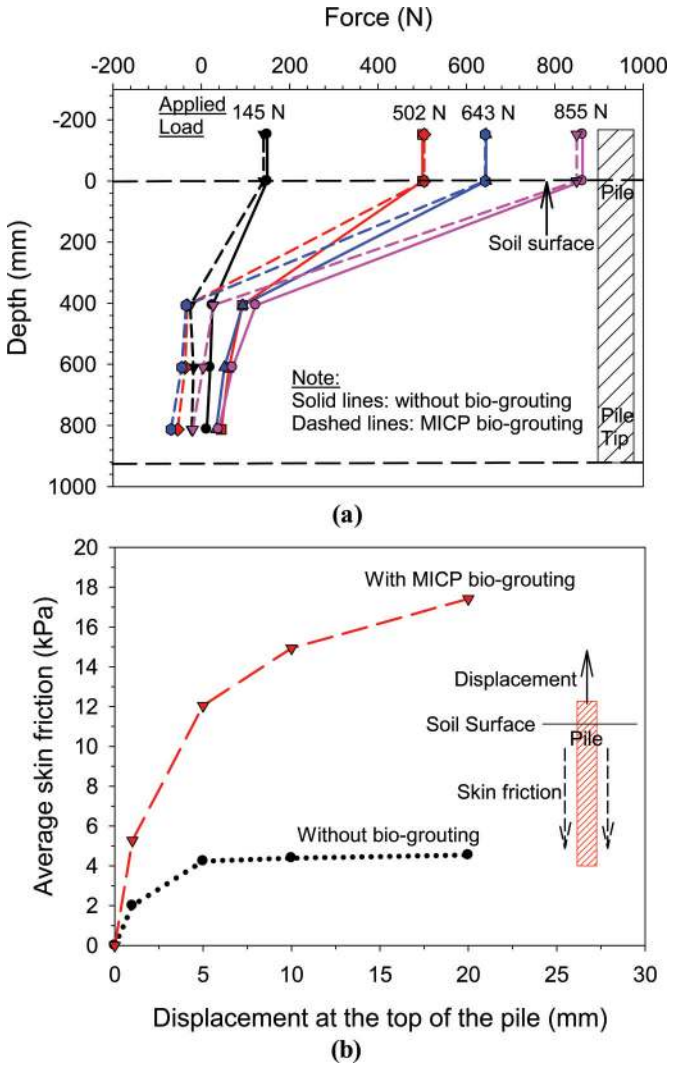

This low infiltration rate was also confirmed by the measured permeability of the pervious concrete samples cut from the pile after the pull-out tests. The average porosity and permeability coefficient of the pile after MICP bio-grouting were 13% and 0.12 cm/s, respectively. When compared to the porosity and permeability coefficient of the cylindrical pervious concrete samples (discussed previously in the section titled "Materials and preparation methods"), the porosity and permeability coefficient of the pervious concrete samples after MICP bio-grouting decreased by 32% and 60%, respectively. It is worth noting that these values could be attributed to the differences in concrete preparation between the pile and samples and (or) due to the bio-clogging formed at the soil–pile interface.

The variation of the S-wave velocities along the pile length during MICP bio-grouting is presented in Fig. 5*a*. At 0 h (before MICP bio-grouting), the S-wave velocities increased linearly with depth. This linearity is similar to the results reported by Fu et al. (2004) from a centrifuge test. During the MICP bio-grouting, S-wave velocities of sensor Nos. 2 and 4 increased immediately upon the initiation of the bio-grouting process, while the S-wave velocities measured by sensor Nos. 7, 1, and 3 showed a delayed increase. At the end of the MICP bio-grouting, the S-wave velocities of sensor Nos. 1, 2, 3, 4, and 7 increased by 1.4, 3.6, 1.4, 1.2, and 1.1 times,

Fig. 9. Contours of (*a*) moisture content and (*b*) $CaCO_3$ content and retrieved pile profile in test No. 2. [Colour online.]

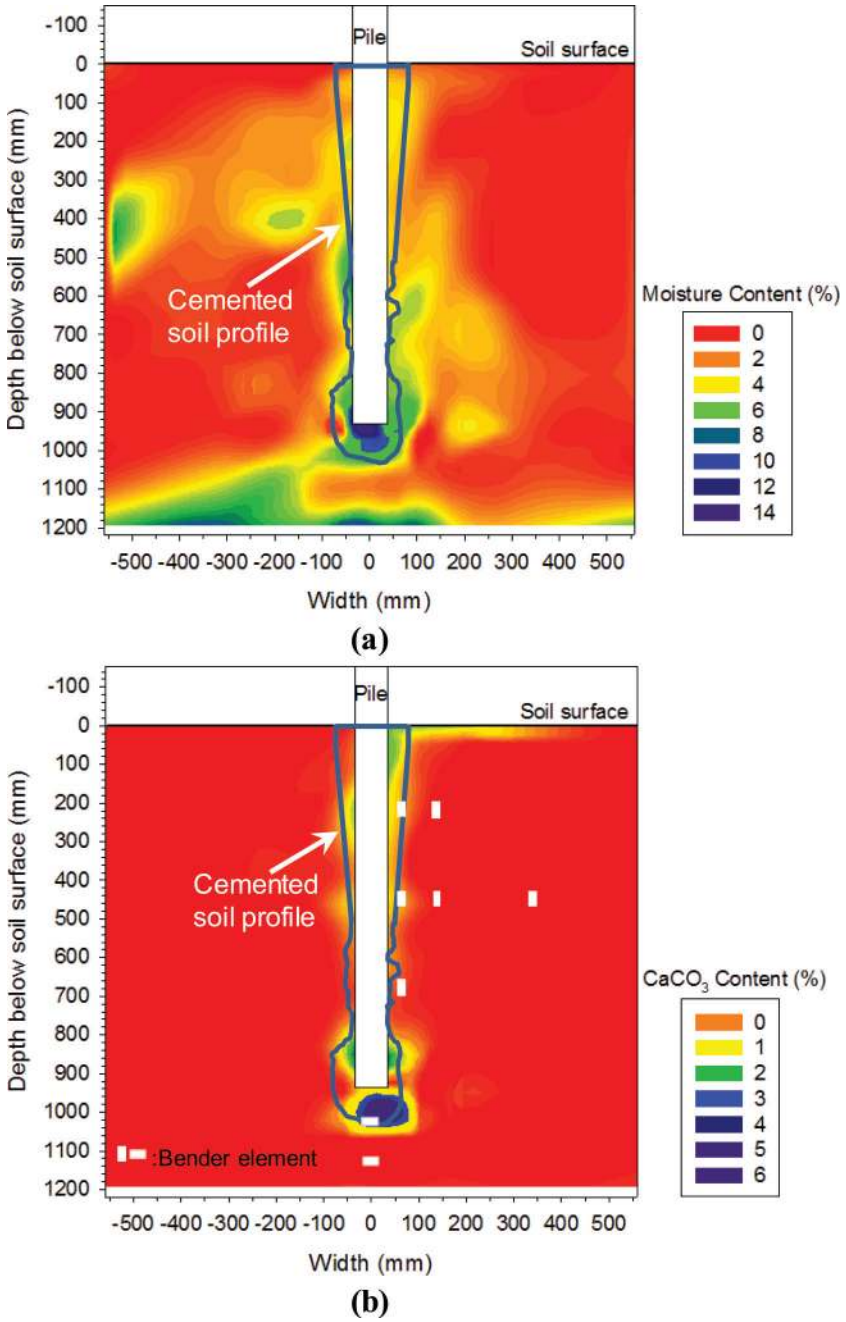

respectively, as compared to their initial S-wave velocities. The variation of the S-wave velocities along the pile length indicates different levels of $CaCO_3$ cementation content in the sand matrix along the pile length and at the pile tip. For example, higher change of S-wave velocity indicates a higher $CaCO_3$ cementation content (Al Qabany et al. 2011; Weil et al. 2011; Lin et al. 2016*b*). Figure 5*a* indicates that $CaCO_3$ contents were highest at the location of sensor No. 2, followed by sensor Nos. 4, 7, 3, and 1.

The S-wave velocities measured by sensor Nos. 2, 6, and 8, which were located at the depth of 458 mm below the soil surface, are shown in Fig. 5*b*. Sensor Nos. 2, 6, and 8 are located at 25, 102, and 305 mm from the pile surface, respectively. During the MICP biogrouting, the S-wave velocity at sensor Nos. 2 and 6 increased by 360% and 30%, respectively, while the S-wave velocities at sensor No. 8 showed almost no change. The variation of the S-wave velocities at soil depth of 458 mm indicates that the $CaCO_3$ precipitated within a limited zone along the pile extending to approximately 102 mm radial distance (location of sensor No. 6) from the pile surface, which is mainly attributed to bio-clogging of soil surrounding the pile as discussed previously.

Load–displacement response

The deformation of the soil surface of test No. 2 during the pull-out loading is shown in Fig. 6*a*. As the axial pull-out load increased, the cemented soil–pile system was pulled out of the surrounding soil, showing a clear cemented zone around the pile. The deformation of the soil surface of test No. 1 (without biogrouting) was negligible as no cemented soil was formed around the pile, and this is discussed in the next paragraph. The measured vertical load–displacement responses at the top of the pile

for test No. 1 (without bio-grouting) and test No. 2 (with bio-grouting) are shown in Fig. 6*b*. The load–displacement responses from both tests showed a linear relationship at the beginning. The initial stiffness (initial slope of load–displacement response) of test No. 2 was 1.1 times higher than that of test No. 1, with a ratio of initial stiffness between the two tests of 2.2. As the load increased, nonlinear plastic responses were observed, followed by large displacement under almost constant load. The ultimate loads for test Nos. 1 and 2 were 919 and 3879 N, respectively, with a ratio of the ultimate loads between MICP-grouted and non-grouted piles of 4.2. This ultimate capacity ratio is similar to the capacity improvements (ratio of 3 to 4 times) for shaft grouted steel piles installed in sand and clayey soils presented by Gouvenot and Gabiax (1975) and Plumbridge and Hill (2001) who investigated bored concrete piles with shaft post-grouting in several types of soils including completely decomposed granites, weathered volcanics, sands, and alluvial deposits.

The deformation of the soil surface surrounding the piles at the end of the tests is shown in Figs. 7*a* and 7*b*. For test No. 2 (with bio-grouting), the cemented sand surrounding the pile was pulled out of the soil with the pile, showing an effective pile diameter increased from 76 to 229 mm, which was not observed in test No. 1 (without bio-grouting). The pile after the pull-out tests was also excavated and inspected as shown in Figs. 7*c* and 7*d*. The pile recovered from test No. 1 (without bio-grouting) showed a pervious concrete surface with small amount of soil filling the voids of the concrete surface. For test No. 2 (with bio-grouting), the approximate zone of cemented sand surrounding the top part of the pile is shown using a dashed line in Fig. 7*d* (because it was unfortunately damaged during handling the pile after the test). The cemented sand matrix at the bottom part of the pile extended the pile effective diameter from 76 mm to approximately 148 mm, and increased the pile length by 76 mm. Based on these results, a limited zone of cemented sand matrix surrounding the pile was achieved, improving the pile response when subjected to axial pull-out loading (Fig. 6*b*). It can be also concluded that unlike test No. 1, the soil–pervious concrete pile system treated with MICP bio-grouting experienced shear failure within the cemented soil along most of the pile length, not along the soil–pile interface.

Load transfer along pile length

Figure 8*a* shows the load transfer along the pile length for both tests. The load at different depths was calculated using the strain gauge measurements and the initial elastic modulus of the pervious concrete composite section including the steel threaded rebar. Loads of 145, 502, 643, and 855 N were selected to compare the load transfer along the pile length in both tests, which represents loading from the initial (linear) stage, through the transition stage, to the ultimate load for test No. 1. The load transfer rates (e.g., slope of the curve or unit friction) for both tests for depths from 0 to 406 mm were highest compared to the deeper soil locations. For soil depths between 0 and 406 mm, the load transfer rate of test No. 2 (with MICP bio-grouting) was higher than that of test No. 1 (without bio-grouting) with maximum difference of 34%. This highest load transfer rate of test No. 2 (between depths of 0–406 mm) is mainly attributed to the higher $CaCO_3$ content and (or) largest cemented zone surrounding the pile, which is confirmed by the maximum S-wave velocities (e.g., bender element No. 2, Fig. 4) and $CaCO_3$ content (discussed further in the paper). The averaged shaft resistance along the pile is plotted against displacement measured at the top of the pile in Fig. 8*b*. The averaged shaft resistance was calculated by averaging the skin frictions between strain gauges along the pile length using the procedure suggested by Troughton et al. (1996). The averaged ultimate shaft resistance along the pile of test No. 2 (with MICP bio-grouting) is 2.8 times higher than that of test No. 1 (without bio-grouting). Similar to bio-grouting, grouting along the shaft of bored piles (diameter of 570 to 900 mm, length of 6 m installed in loose to dense sand) as reported by Stocker (1983) and Plumbridge and Hill (2001) produced an increase of the shaft resistance by up to 73%, which is smaller than the improvement achieved by MICP bio-grouting. This difference could be attributed to the encountered sand conditions, grouting process, and physical characteristics of the piles used.

Fig. 10. $CaCO_3$ contents as a function of distances to pile at several soil depths. [Colour online.]

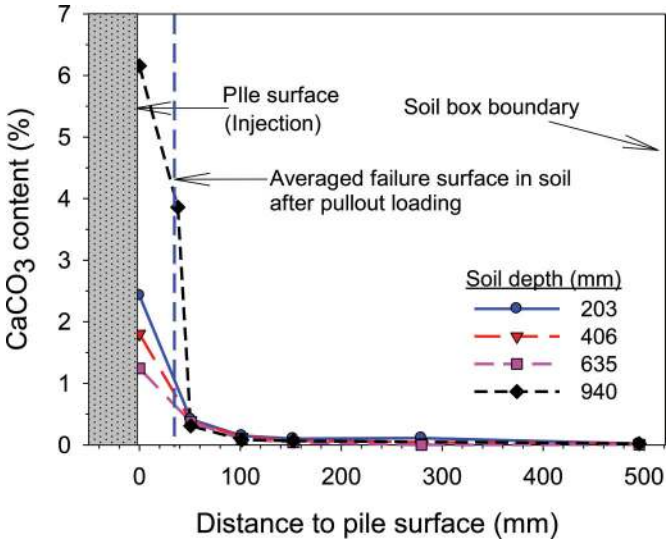

Moisture and calcium carbonate contents in sand box

Soil samples were collected across the soil box in both test No. 1 without bio-grouting (40 samples) and test No. 2 with MICP bio-grouting (270 samples). The measured moisture contents from test No. 2 are plotted in Fig. 9*a*, which also includes the profile of the cemented zone around the pile. The highest moisture contents were located adjacent to the pile and at the bottom of the soil box. They ranged from 0% to 13.9%, with an average of 4.9% near the soil–pile interface, which is similar to the moisture content measured from test No. 1. The highest moisture content was observed at the tip of the pile and in the cemented sand zone due to bio-clogging.

For test No. 2, the 270 samples were utilized to determine the $CaCO_3$ content. A cross section of the measured $CaCO_3$ content in the soil box is shown in Fig. 9*b*. The $CaCO_3$ precipitated only around the pile, extending the cemented zone from the pile surface to approximately 102 mm. It is important to note that the $CaCO_3$ contents at shallow soil depth (0 to 406 mm) and below the pile tip were higher than the remaining parts along the pile length, which results in highest load transfer rate and higher S-wave velocities. The observed higher $CaCO_3$ content at both locations could be attributed to the media flow pattern (either flow to the tip of the pile or radially from the pile to surrounding soil), which is controlled by the flow channel distribution in the cast pervious concrete pile. The pile profile after soil removal (i.e., showing the pile and soil cemented to it after the test) is also shown in Fig. 9*b*. Based on the pile profile after soil removal and the $CaCO_3$ content contour, the shear failure of the pile–soil system occurred in the cemented sand zone (not at the soil–pile interface). The bender element sensors located within the $CaCO_3$ cemented zone (Fig. 9*b*) indicated significant measurement changes as shown in Figs. 4 and 5, confirming the measuring validity of bender elements.

The $CaCO_3$ contents at four depths below the soil surface along the pile length are presented in Fig. 10. The distribution of $CaCO_3$ content was not uniform along the soil–pile interface. The $CaCO_3$ content at a depth of 203 mm was highest and then started de-

Fig. 11. SEM images of sand matrix without MICP treatment and with MICP bio-grouting at different soil depths at the soil–pile interface (i.e., pile surface). [Colour online.]

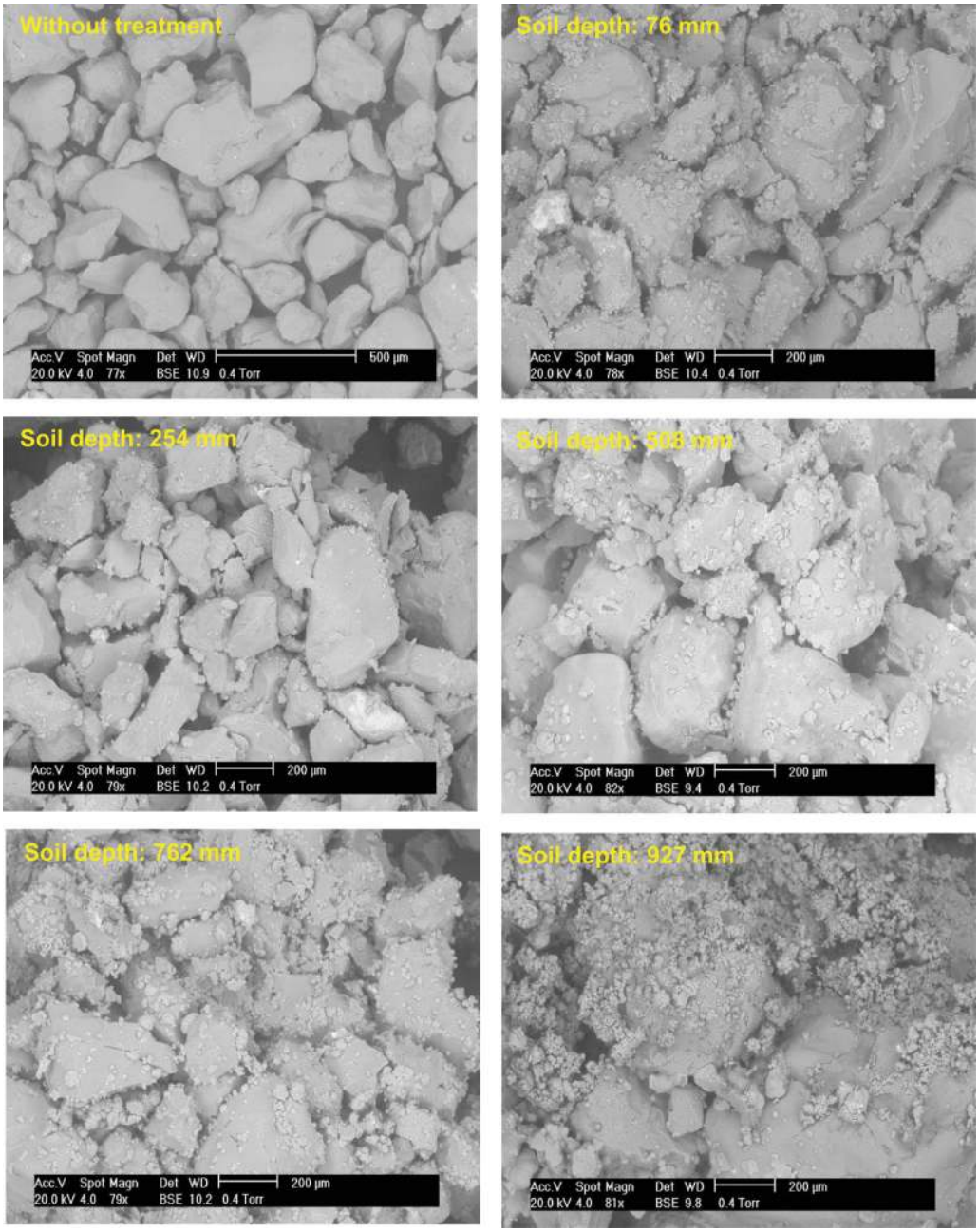

creasing along the pile length, which caused the higher load transfer rate at shallow depth shown in Fig. 8*a*. The average $CaCO_3$ content along the soil–pile interface (i.e., pile surface) at different depths was 1.8%. However, the $CaCO_3$ content (6.2%) at the pile tip (depth 940 mm) was 2.4 times higher than the average $CaCO_3$ content at the soil–pile interface. In addition, it is worth noting that the distribution of $CaCO_3$ as a function of distance from the pile (Fig. 10) matched the S-wave velocity profile shown in Fig. 5*b*. The measured $CaCO_3$ contents indicates that a small $CaCO_3$-cemented zone around the pile was achieved in test No. 2. The approximate average location of shear failure surface for test No. 2 was approximately at 36 mm from the pile surface (Fig. 7 and labelled in Fig. 10), demonstrating that the $CaCO_3$ content at the failure interface ranged from 0.6% to 1.2%.

Crystal characteristics of $CaCO_3$ in sand matrix

SEM images of sand samples collected around the pile surface are presented in Fig. 11 and $CaCO_3$ deposition is clearly evident after MCIP treatment. Two main types of $CaCO_3$ morphologies, rhomboidal calcite and spherical vaterite crystals, were observed in these images. It is important to note that the $CaCO_3$ morphology is determined mainly by the urea hydrolysis rate (van Paassen 2009; Lin et al. 2016*a* and 2016*b*). However, it is still not clearly understood if the type of $CaCO_3$ crystals affects the shaft resistance of the bio-grouted pervious concrete piles. In addition, it was observed that the $CaCO_3$ deposition in the bar sand was both grain coating (coating sand particles) and matrix supporting (grows from particle surface into pore space creating a cementa-

tion bridge between soil grains), which are the main types of $CaCO_3$ crystals observed in the pore space of the sand matrix (Lin et al. 2016*b*).

Field applications

The extension of MICP bio-grouting treatment to field scale depends on the ease of movement (transport) of microbes in the soil matrix, which is controlled by the size of pore throat (Mitchell and Santamarina 2005; DeJong et al. 2010). Most available soil test results with MICP treatment were limited to fine poorly graded and coarser graded sands that have large pore throats allowing microbial movement before precipitating $CaCO_3$ (DeJong et al. 2006; Whiffin et al. 2007; van Paassen 2009; Al Qabany and Soga 2013; Montoya and DeJong 2015; Lin et al. 2016*b*). Therefore, changing the void ratio in the tests may affect the microbial movement and efficiency of MICP. The effect of MICP on mechanical properties of different sands at a range of relative densities (from 30% to 100%) was reported by Chou et al. (2011), Al Qabany and Soga (2013), and Tsukamoto and Oda (2013). These studies concluded that sands prepared at higher relative density also showed higher peak shear strength and higher rate of strength increase as calcium carbonate precipitation increases. However, these studies utilized pressure to inject solutions into soil samples, which differs from the percolation process used in our laboratory experiments. Therefore, the effect of void ratio on the efficiency of MICP for field applications with percolation (not pressure injection) may require further validation. It is also worth noting that the assessment of the efficiency of pressurized cement grouting along the shaft of concrete piles with different diameters was reported and compared by Troughton et al. (1996). It was concluded that the calculated skin friction after shaft grouting decreased with increasing pile diameter. This could be attributed to pressures applied during grouting or to limited penetration of cementation in surrounding soils. However, permeable ground improvement piles have high permeability (does not require pressure) along the pile length, which enables MICP bio-grouting to achieve cementation in the surrounding soil. Furthermore, MICP bio-grouting uses lower viscosity solution than cement grout, which is expected to produce improved cemented zone in the surrounding soil. Thus, it is possible that higher shaft resistance could be achieved with MICP bio-grouting treatment in the field. However, this requires full-scale field validation, which the research team plan to perform in the future and will discuss those in more detail in future papers.

Summary and conclusions

This paper investigated the enhanced axial pull-out response of permeable ground improvement piles using MICP bio-grouting. Two instrumented pervious concrete pile tests without and with MICP bio-grouting (test Nos. 1 and 2, respectively) were performed at the Soil-Structure Interaction Facility at Lehigh University. The measured pile responses, S-wave velocities, moisture and $CaCO_3$ contents, and crystal characteristics of $CaCO_3$ were analyzed. Based on the results presented in this paper, the following conclusions are drawn:

1. The S-wave velocities of sensors located at 102 mm distance from the pile surface and 203 mm below the pile tip increased by an average of 1.5 times compared to the measurements before bio-grouting due to the formation of $CaCO_3$ cemented soil zone around the pile. The infiltration rate of the soil–pile system concurrently decreased by up to 98%, confirming the clogging of the soil surrounding MICP injection points. The S-wave velocity and infiltration rate can be used to monitor future field tests of permeable piles with bio-grouting.
2. The S-wave velocity at sensor Nos. 2, 6, and 8 increased by 360%, 30%, and 0%, respectively, indicating that the cementation decreases with distance from the pile and that the cemented soil zone surrounding the pile was limited to radial distance approximately 102 mm to the pile surface.
3. The ratios of the stiffness (initial slope) of the load–displacement response and the ultimate load between test No. 2 (with MICP bio-grouting) and test No. 1 (without bio-grouting) were 2.2 and 4.2, respectively. This stiffness and load capacity improvement confirmed the significant effects of limited zone bio-grouting on enhancing the pull-out response of permeable piles.
4. The load transfer rate of test No. 2 (with MICP bio-grouting) was up to 34% higher than that of test No. 1 (without bio-grouting). The averaged ultimate shaft resistance along the pile of test No. 2 was 2.8 times higher than that of test No. 1 without bio-grouting. The observed improvement of the load transfer and shaft resistance confirmed the pile capacity improvement using MICP bio-grouting.
5. Similar to the S-wave distribution, the $CaCO_3$ contents decreased with distance from the pile and indicated a limited cemented soil zone surrounding the pile. The precipitation of $CaCO_3$ was not uniform around the pile.
6. Based on the pile profile after soil removal (the pile and soil cemented to it after the test), the $CaCO_3$ content at the failure surface in the cemented soil–pile system ranged from 0.6% to 1.2%.
7. Both calcite and vaterite crystals were observed around the pile with the main types of $CaCO_3$ distributions in the bar sand were grain coating and matrix supporting.

Acknowledgements

The authors would like to acknowledge the support of the Civil, Mechanical, and Manufacturing Innovation (CMMI) Division at National Science Foundation (No. 1233566). The research team would like to acknowledge the efforts of several graduate students, including Mathu Davis, Suguang Xiao, and Lusu Ni. In addition, the authors would like to acknowledge the help of Edward Tomlinson and Darrick Fritchman, instrumentation and system specialists at Lehigh University's Advanced Technology for Large Structural Systems (ATLSS) Engineering Research Center.

References

Al Qabany, A., and Soga, K. 2013. Effect of chemical treatment used in MICP on engineering properties of cemented soils. Géotechnique, **63**(4): 331–339. doi:10.1680/geot.SIP13.P.022.

Al Qabany, A., Mortensen, B., Martinez, B., Soga, K., and DeJong, J. 2011. Microbial carbonate precipitation: correlation of S-wave velocity with calcite precipitation. *In* Proceedings of the ASCE Geo-Frontiers 2011 Conference. ASCE, Reston, Va. pp. 3993–4001.

Altaee, A., and Fellenius, B.H. 1994. Physical modeling in sand. Canadian Geotechnical Journal, **31**(3): 420–431. doi:10.1139/t94-049.

ASTM. 2009*a*. Standard test method for maximum index density and unit weight of soils using a vibratory table. ASTM standard D4253. ASTM, West Conshohocken, Pa.

ASTM. 2009*b*. Standard test method for minimum index density and unit weight of soils and calculation of relative density. ASTM standard D4254. ASTM, West Conshohocken, PA.

ASTM. 2009*c*. Standard test method for compressive strength of cylindrical concrete specimens. ASTM standard C39, West Conshohocken, Pa.

ASTM. 2009*d*. Standard test method for density and void content of freshly mixed pervious concrete. ASTM standard C1688. ASTM, West Conshohocken, Pa.

ASTM. 2009*e*. Standard test method for splitting tensile strength of cylindrical concrete specimens. ASTM standard. ASTM C496, West Conshohocken, Pa.

ASTM. 2009*f*. Standard test method for infiltration rate of in place pervious concrete. ASTM standard C1701. ASTM, West Conshohocken, Pa.

ASTM. 2009*g*. Standard test method for deep foundations under static axial tensile load. D3689. ASTM, West Conshohocken, PA.

ASTM. 2011. Standard practice for classification of soils for engineering purposes (Unified Soil Classification System). ASTM standard D2487. American Society for Testing and Materials, West Conshohocken, Pa. doi:10.1520/D2487-11.

Been, K., and Jefferies, M.G. 1985. A state parameter for sands. Géotechnique, **35**: 99–112. doi:10.1680/geot.1985.35.2.99.

Bruce, D.A. 1986*a*. Enhancing the performance of large diameter piles by grouting: Part 1. Ground Engineering, **19**(4): 9–15.

Bruce, D.A. 1986*b*. Enhancing the performance of large diameter piles by grouting: Part 2. Ground Engineering, **19**(5): 1121–1126.

Burbank, M., Weaver, T., Lewis, R., Williams, T., Williams, B., and Crawford, R.

2013. Geotechnical tests of sands following bioinduced calcite precipitation catalyzed by indigenous bacteria. Journal Geotechnical Geoenvironmental Engineering, **139**(6): 928–936. doi:10.1061/(ASCE)GT.1943-5606.0000781.

Cheng, L., and Cord-Ruwisch, R. 2013. Upscaling effects of soil improvement by microbially induced calcite precipitation by surface percolation. Geomicrobiology Journal, **31**(5): 396–406. doi:10.1080/01490451.2013.836579.

Chou, C., Seagren, E.A., Aydilek, A.H., and Lai, M. 2011. Biocalcification of sand through ureolysis. Journal of Geotechnical and Geoenvironmental Engineering, **137**(12): 1179–1189. doi:10.1061/(ASCE)GT.1943-5606.0000532.

Dapp, S., and Brown, D. 2010. Evaluation of base grouted drilled shafts at the Audubon Bridge. *In* Proceedings of GeoFlorida 2010, Advances in Analysis, Modeling & Design. ASCE, Reston, Va. pp. 1553–1562.

Dapp, S.D., and Mullins, G. 2002. Pressure grouting drilled shaft tips: full-scale research investigation for silty and shelly sands. *In* Proceedings of Deep Foundations 2002, Geotechnical Special Publication No. 116. ASCE, Reston, VA, pp. 335–350.

DeJong, J., Fritzges, M., and Nüsslein, K. 2006. Microbially induced cementation to control sand response to undrained shear. Journal of Geotechnical and Geoenvironmental Engineering, **132**(11): 1381–1392. doi:10.1061/(ASCE)1090-0241(2006)132:11(1381).

DeJong, J.T., Mortensen, B.M., Martinez, B.C., and Nelson, D.C. 2010. Bio-mediated soil improvement. Ecology Engineering, **36**(2): 197–210. doi:10.1016/j.ecoleng.2008.12.029.

Dejong, J.T., Soga, K., Kavazanjian, E., Burns, S., van Paassen, L.A., Al Qabany, A., et al. 2013. Biogeochemical processes and geotechnical applications: progress, opportunities and challenges. Géotechnique, **63**(4): 287–301. doi:10.1680/geot.SIP13.P.017.

Fattahpour, V., Baudet, B.A., and Sze, J.W. 2015. Laboratory investigation of shaft grouting. *In* Proceedings of the ICE - Geotechnical Engineering, **168**(1): 65–74. doi:10.1680/geng.13.00130.

Feng, K., and Montoya, B.M. 2015. Influence of confinement and cementation level on the behavior of microbial-induced calcite precipitated sands under monotonic drained loading. Journal of Geotechnical and Geoenvironmental Engineering, **142**(1). doi:10.1061/(ASCE)GT.1943-5606.0001379.

Ferris, F.G., Stehmeier, L.G., Kantzas, A., and Mourits, F.M. 1996. Bacteriogenic mineral plugging. Journal Canadian Petroleum Technology, **35**(8): 56–61.

Fu, L., Zeng, X., and Figueroa, J.L. 2004. Shear wave velocity measurement in centrifuge using bender elements. International Journal of Physical Modelling in Geotechnics, **2**: 1–11. doi:10.1680/ijpmg.2004.040201.

Gouvenot, D., and Gabiax, F.D. 1975. A new foundation technique using piles sealed by concrete under high pressure. *In* Proceedings of the 7th Annual Offshore Technology Conference. Houston, Tex. pp. 641–656.

Ishihara, K., Verdugo, K., and Acacio, A. A. 1991. Characterization of cyclic behavior of sand and post-seismic stability analyses. *In* Proceedings of the 9th Asian Regional Conference on Soil Mechanics and Foundation Engineering. Bangkok. Vol. 2, pp. 45–67.

Ivanov, V., and Chu, J. 2008. Applications of microorganisms to geotechnical engineering for bioclogging and biocementation of soil in situ. Reviews in Environmental Science and BioTechnology, **7**(2): 139–153. doi:10.1007/s11157-007-9126-3.

Janbu, N. 1963. Soil compressibility as determined by oedometer and triaxial tests. *In* Proceedings of European Conference on Soil Mechanics and Foundation Engineering, Wiesbaden, Germany. Vol. 1, pp. 19–25.

Joer, H.A., Randolph, M.F., and Gunasena, U. 1998. Experimental modeling of the shaft capacity of grouted driven piles. Geotechnical Testing Journal, **21**(3): 159–168. doi:10.1520/GTJ10889J.

Lin, H., Suleiman, M., Jabbour, H., and Brown, D. 2015. Enhancement of pervious concrete pile subjected to uplift load using microbial induced carbonate precipitation. *In* Proceedings of IFCEE 2015. ASCE, Reston, Virginia. pp. 775–783.

Lin, H., Suleiman, M.T., Jabbour, H.M., Brown, D.G., and Kavazanjian, E. 2016*a*. Enhancing the axial compression response of pervious concrete ground improvement piles using bio-grouting [online]. Journal of Geotechnical and Geoenvironmental Engineering, doi:10.1061/%28ASCE%29GT.1943-5606.0001515.

Lin, H., Suleiman, M.T., Brown, D.G., and Kavazanjian, E. 2016*b*. Mechanical behavior of sands treated by microbially induced carbonate precipitation (MICP). Journal of Geotechnical and Geoenvironmental Engineering, **142**(2). doi:10.1061/(ASCE)GT.1943-5606.0001383.

Mitchell, J.K., and Santamarina, J.C. 2005. Biological considerations in geotechnical engineering. Journal of Geotechnical and Geoenvironmental Engineering, **131**(10). doi:10.1061/(ASCE)1090-0241(2005)131:10(1222).

Montoya, B., and DeJong, J. 2015. Stress-strain behavior of sands cemented by microbially induced calcite precipitation. Journal of Geotechnical and Geoenvironmental Engineering, **141**(6). doi:10.1061/(ASCE)GT.1943-5606.0001302.

Mortensen, B.M., Haber, M.J., DeJong, J.T., Caslake, L.F., and Nelson, D.C. 2011. Effects of environmental factors on microbial induced calcium carbonate precipitation. Journal of Applied Microbiology, **111**(2): 338–349. doi:10.1111/j.1365-2672.2011.05065.x.

Mullins, G., Winters, D., and Dapp, S. 2006. Predicting end bearing capacity of post-grouted drilled shaft in cohesionless soils. Journal of Geotechnical and Geoenvironmental Engineering, **132**(4): 478–487. doi:10.1061/(ASCE)1090-0241(2006)132:4(478).

Ni, L., Suleiman, M.T., and Raich, A. 2016. Behavior and soil-structure interaction of pervious concrete ground improvement piles under lateral loading. Journal of Geotechnical and Geoenvironmental Engineering, **142**(2). doi:10.1061/(ASCE)GT.1943-5606.0001393.

Nunez, I.L. 1988. Driving and tension loading of piles in sand on a centrifuge. *In* Proceedings of the International Conference Centrifuge 88, Paris. *Edited by* Corté, J.F. Balkema, Rotterdam. pp. 353–362.

Ovensen, N.K. 1979. The scaling law relationship – panel discussion. *In* Proceedings of the 7th European Conference on Soil Mechanics and Foundation Engineering. Brighton, UK. pp. 319–323.

Plumbridge, G.D., and Hill, S.J. 2001. Performance of shaft grouted piles and barrettes. *In* Proceedings of the 14th Southeast Asian Geotechnical Conference: Geotechnical Engineering: Meeting Society's Needs. A. A. Balkema Publishers, Netherlands. pp. 407–412.

Ruiz, M., and Pando, M. 2009. Load transfer mechanisms of tip post-grouted drilled shafts in sand. *In* Proceedings of Contemporary Topics in Deep Foundations. ASCE, Reston, Va. pp. 23–30.

Soon, N., Lee, L., Khun, T., and Ling, H. 2014. Factors affecting improvement in engineering properties of residual soil through microbial-induced calcite precipitation. Journal of Geotechnical and Geoenvironmental Engineering, **140**(5). doi:10.1061/(ASCE)GT.1943-5606.0001089.

Stocker, M.F. 1983. The influence of post grouting on the load bearing capacity of bored piles. *In* Proceedings of the 8th European Conference on Soil Mechanics and Foundation Engineering, Helsinki. Paper 2.12.

Stocks-Fischer, S., Galinat, J.K., and Bang, S.S. 1999. Microbiological precipitation of $CaCO_3$. Soil Biology and Biochemistry, **31**(11): 1563–1571. doi:10.1016/S0038-0717(99)00082-6.

Suer, P., Hallberg, N., Carlsson, C., Bendz, D., and Holm, G. 2009. Biogrouting compared to jet grouting: environmental (LCA) and economical assessment. Journal of Environmental Science and Health Part A, **44**(4): 346–53. doi:10.1080/10934520802659679.

Suleiman, M.T., Ni, L., and Raich, A. 2014. Development of pervious concrete pile ground-improvement alternative and behavior under vertical loading. Journal of Geotechnical and Geoenvironmental Engineering, **140**(7). doi:10.1061/(ASCE)GT.1943-5606.0001135.

Thiyyakkandi, S., McVay, M., Bloomquist, D., and Lai, P. 2013. Measured and predicted response of a new jetted and grouted precast pile with membranes in cohesionless soils. Journal of Geotechnical and Geoenvironmental Engineering, **139**(8): 1334–1345. doi:10.1061/(ASCE)GT.1943-5606.0000860.

Troughton, V.M., Stocker, M., and Thompson, P.A. 1996. Base and shaft grouted piles. *In* Proceedings of the Institution of Civil Engineers - Geotechnical Engineering, **119**(3): 186–192. doi:10.1680/igeng.1996.28511.

Tsukamoto, M., and Oda, K. 2013. Influence of relative density on microbial carbonate precipitation and mechanical properties of sand. *In* Proceedings of the 18th International Conference on Soil Mechanics and Geotechnical Engineering. Paris. pp. 2613–2616.

van Paassen, L.A. 2009. Biogrout ground improvement by microbially induced carbonate precipitation. PhD thesis, Delft University of Technology.

van Paassen, L., Ghose, R., van der Linden, T., van der Star, W., and van Loosdrecht, M. 2010. Quantifying biomediated ground improvement by ureolysis: large-scale biogrout experiment. Journal of Geotechnical and Geoenvironmental Engineering, **136**(12): 1721–1728. doi:10.1061/(ASCE)GT.1943-5606.0000382.

Vanitha, L., Patra, N.R., and Chandra, S. 2007. Uplift capacity of pile group anchors. Geotechnical and Geological Engineering, **25**(3): 339–347. doi:10.1007/s10706-006-9114-3.

Weil, M.H., DeJong, J.T., Martinez, B.C., and Mortensen, B.M. 2011. Seismic and resistivity measurements for real-time monitoring of microbially induced calcite precipitation in sand. Geotechnical Testing Journal, **35**(2): 1–11.

Whiffin, V.S., van Paassen, L.A., and Harkes, M.P. 2007. Microbial carbonate precipitation as a soil improvement technique. Geomicrobiology Journal, **24**(5): 417–423. doi:10.1080/01490450701436505.